

# Model-Informed Generative Adversarial Network (MI-GAN) for Learning Optimal Power Flow

Yuxuan Li<sup>1</sup>, Chaoyue Zhao<sup>2</sup>, and Chenang Liu<sup>1\*</sup>

<sup>1</sup>The School of Industrial Engineering & Management, Oklahoma State University, Stillwater, OK

<sup>2</sup>Department of Industrial and Systems Engineering, University of Washington, Seattle, WA

\*Corresponding author: [chenang.liu@okstate.edu](mailto:chenang.liu@okstate.edu)

**Abstract--** The optimal power flow (OPF) problem, as a critical component of power system operations, becomes increasingly difficult to solve due to the variability, intermittency, and unpredictability of renewable energy brought to the power system. Although traditional optimization techniques, such as stochastic and robust optimization approaches, could be used to address the OPF problem in the face of renewable energy uncertainty, their effectiveness in dealing with large-scale problems remains limited. As a result, deep learning techniques, such as neural networks, have recently been developed to improve computational efficiency in solving large-scale OPF problems. However, the feasibility and optimality of the solution may not be guaranteed. In this paper, we propose an optimization model-informed generative adversarial network (MI-GAN) framework to solve OPF under uncertainty. The main contributions are summarized into three aspects: (1) to ensure feasibility and improve optimality of generated solutions, three important layers are proposed: feasibility filter layer, comparison layer, and gradient-guided layer; (2) in the GAN-based framework, an efficient model-informed selector incorporating these three new layers is established; and (3) a new recursive iteration algorithm is also proposed to improve solution optimality. The numerical results on IEEE test systems show that the proposed method is very effective and promising.

**Index Terms--** generative adversarial network (GAN), model-informed generation, optimal power flow (OPF), power system, recursive iteration

## 1. INTRODUCTION

The national electricity sector has witnessed a dramatic change in renewable energy penetration in recent years, and its share is expected to continue growing rapidly in the next few decades. On a federal level, the U.S. Energy Information Administration (EIA) predicts that renewable energy resources will provide 38% of electricity energy by 2050, with solar and wind energy accounting for 17.5% and 12.54%, respectively [1]. With such a high renewable energy penetration, it is critical and urgent for power system operators to learn how to operate power systems effectively and securely in the face of high variability, intermittency, and unpredictability of renewable energy output.

Optimal power flow (OPF), as an essential component of power system operations and management, aims to minimize the total generation cost while satisfying a series of system constraints and operational requirements, achieving economic power system operation in day-ahead and real-time markets. As a key building block of many complex power system problems, the OPF problem under renewable energy uncertainty has been

extensively studied in recent years. The most common approach to formulating the OPF problem with renewable energy uncertainties is stochastic OPF (e.g., [2, 3], among others), in which the uncertain renewable energy output is characterized by a finite number of scenarios, or is assumed to follow a particular probability distribution, and then sampling approaches are typically used to finalize the formulation. The robust optimization approach (e.g., [4, 5] among others) is another traditional approach to addressing the OPF problem with renewable energy uncertainties. Its key idea is to construct an OPF solution that is optimal for the worst-case realization of renewable energy output in a predefined uncertainty set. Recently, the distributionally robust OPF problem (e.g., [6, 7] among others) has also been proposed to hybrid stochastic and robust approaches, by considering the worst-case distribution of renewable energy output. The obtained OPF decisions are expected to be less conservative than the ones from the robust approach and more reliable than the ones from the stochastic approach.

Despite the great success for these approaches in effectively addressing OPF problem with the renewable energy uncertainty, the practical use of these methods remains limited due to scalability issues for large-scale power systems. The staggering advances obtained in deep learning in recent years make it possible to quickly find the optimal strategy of computationally intensive power system optimization problems. Over the last decade, various deep learning approaches have been used to address OPF problems and can be divided into two major categories. One is based on the training of neural network, such as convolutional neural networks (CNN) [8, 9] and graph neural networks (GCN) [10, 11], to learn a high-dimensional mapping between net load (i.e., load minus renewable energy output) inputs and corresponding dispatch and transmission decisions from historical records. However, the solutions they provide are not trustworthy in real-world system operation, as the solution feasibility or optimality cannot be guaranteed. The other direction is to utilize the deep reinforcement learning (RL) to generate instantaneous OPF decisions corresponding to the real-time change of net load inputs [12, 13]. However, since RL algorithms are known to learn by trial and error, the obtained OPF controls also lack a safety guarantee. In addition, a commonality among all these methods is that they primarily depend on supervised learning techniques and massive simulations obtained ahead of time to train the neural networks, which results in sample inefficiency.

To address the OPF problems under net load uncertainty, we propose a novel optimization model-informed generative adversarial network (MI-GAN) framework in this paper. The emerging generative adversarial network (GAN) was first proposed by Goodfellow [14]. It was originally designed for image augmentation [15], but it is now applied to a variety of fields, including manufacturing [16], business fraud detection [17], and healthcare [18]. GAN trains two networks, generator  $G$  and discriminator  $D$ , based on a minimax game for  $V(D, G)$  shown in Eq. (1).

$$\begin{aligned} \min_G \max_D V(D, G_m) = & \mathbb{E}_{\mathbf{x} \sim P_{\text{data}}(\mathbf{x})} [\log(D(\mathbf{x}))] \\ & + \mathbb{E}_{\mathbf{z} \sim P_{\mathbf{z}}(\mathbf{z})} [\log(1 - D(G(\mathbf{z})))] \end{aligned} \quad (1)$$

where  $G$  generates artificial samples  $G(\mathbf{z})$  based on noise  $\mathbf{z}$  generated at random. Then  $D$  differentiates between artificial samples  $G(\mathbf{z})$  and actual samples  $\mathbf{x}$ . Following that,  $G$  and  $D$  compete against each other. The ultimate goal of GAN is to make it nearly impossible for  $D$  to tell whether the generated samples are actual data or artificial data. Then the artificial data is sufficiently similar to the actual data [14]. In this way, even when the data is complex and high-dimensional, a GAN-based framework can learn the underlying relationships among the data. Deep convolutional GAN (DCGAN) [19], for example, could generate high-dimensional images with competitive performance by incorporating a convolutional neural network (CNN). Furthermore, conditional GAN (CGAN) [20] makes the training process more stable and controllable by using target classification variables as a reference in iterations. GAN-based approaches, in particular, could be used in optimization, though few existing GAN-based approaches have been developed for this purpose. In the GAN-based framework, the output of  $G$  could be generated solutions, whereas the actual data could be the historical solutions, i.e., the actual solutions centered on the optimal solution. As a result, the distribution of generated solutions could gradually approach to the distribution of historical solutions. Then the optimal solution could be obtained. However, if the historical solutions do not exist or are not centered on optimal solutions, updating the generated solutions to move forward to the optimal solution becomes a challenge. Besides, ensuring the generated solutions by  $G$  to satisfy the constraints is difficult.

In this paper, inspired by the previous work of augmented time-regularized GAN (ATR-GAN) [15], we apply the proposed model-informed GAN (MI-GAN) framework to address the direct current OPF (DC-OPF) problem under net load. The proposed novel MI-GAN differs from traditional deep learning approaches in two major ways.

First, rather than learning the mapping between the net load and control decisions, the GAN architecture can learn the underlying distribution of optimal OPF decisions and directly generate corresponding solutions for different realizations of net load. In this manner, solutions can be fast generated from the learned distribution without involving the neural network. Second, unlike traditional neural network-based methods, including the conventional GAN, which ignore the model structure, the proposed MI-GAN incorporates the model

constraints and gradient information during the training of GAN in the following ways: (i) to ensure the feasibility, a new feasibility filter layer is added to the model-informed selector to check if the solution meets all the physical constraints. If not, the solution will be filtered out, and this information will be synthesized to MI-GAN to discourage similar solutions from being generated again; (ii) to utilize the information from the objective function and further improve the solution optimality, the resultant objective function value and gradient information are also integrated into the generator training to guide MI-GAN to search for better solutions; and (iii) MI-GAN does not require a large number of data samples, since it can guide the search and improve its solution quality using self-generated data.

To summarize, the contributions of the proposed method consist of three parts:

- i) To address OPF problems with net load uncertainty, a new GAN-based learning framework, MI-GAN, is proposed. Three critical new layers are designed and integrated to ensure the feasibility and improve the optimality of generated solutions: the feasibility filter layer, the comparison layer, and the gradient-guided layer.
- ii) An efficient model-informed selector combined with the three new layers are developed.
- iii) A new recursive iteration algorithm is also proposed to further reduce the bias between selected solutions and optimal solutions.

Furthermore, the performance of the proposed MI-GAN framework is investigated using multiple testing cases, and the results show the supreme performance and efficiency of our proposed method compared with optimization and the state-of-art AI-optimization approaches on OPF problems. The rest of the work is organized as follows: In Sec. 2, the general mathematical formulation of the DC-OPF problem is presented. In Sec. 3, model-informed GAN is proposed to solve the DC-OPF problem under uncertainty. Numerical results and comparisons on IEEE test systems are presented in Sec. 4 to demonstrate the effectiveness of the proposed method. Finally, conclusions are drawn in Sec. 5.

## 2. THE OPTIMAL POWER FLOW PROBLEM

In the following DC-OPF problem, we assume that the voltages are constants at all buses. Then there are two groups of variables: the power generation,  $\mathbf{p}_g$ , and the power voltage phase angles,  $\boldsymbol{\theta}$ . Denote  $n_b$  and  $n_g$  as the numbers of buses and power generators respectively. Then  $\mathbf{p}_g = \{p_{g1}, p_{g2}, \dots, p_{gn_g}\}$  where  $p_{gi}$  is the power generation for generator  $i$ , and  $\boldsymbol{\theta} = \{\theta_1, \theta_2, \dots, \theta_{n_b}\}$  where  $\theta_i$  is the phase angle for bus  $i$ . In addition, denote that the power load is  $\mathbf{p}_d$  and there are  $n_d$  buses that have the net load. Based on the lines between different buses, the power output could be sent following one matrix  $\mathbf{M}_g$  and the power load could be received following another matrix  $\mathbf{M}_d$ . The size of  $\mathbf{M}_g$  is  $n_b \times n_g$  while the size of  $\mathbf{M}_d$  is  $n_b \times n_d$ . Based on the notations, the formulation of the DC-OPF problem is shown in Eq. (2)-(5).

$$\min_{\mathbf{p}_g, \theta} \mathbf{c}^T \mathbf{p}_g \quad (2)$$

$$\text{s. t. } \mathbf{M}_g \mathbf{p}_g - \mathbf{M}_d \mathbf{p}_d = \mathbf{B}_{\text{bus}} \theta \quad (3)$$

$$\mathbf{p}_{\text{line}}^{\min} \leq \mathbf{B}_{\text{line}} \theta \leq \mathbf{p}_{\text{line}}^{\max} \quad (4)$$

$$\mathbf{p}_g^{\min} \leq \mathbf{p}_g \leq \mathbf{p}_g^{\max} \quad (5)$$

Eq. (2) is the function to minimize the power generation cost where the coefficients used to calculate the cost for all the generators are denoted as  $\mathbf{c}$ . Following that, the minimization is constrained by the power balance equation, the transmission line capacity constraints, and the generation operation limits. Eq. (3) means that the power output should balance the net load, and the in- and out-going flows for all the buses where  $\mathbf{B}_{\text{bus}}$  is the bus admittance matrix. In addition, Eq. (4) shows the minimum and maximum active line flow limits based on the line admittance matrix  $\mathbf{B}_{\text{line}}$ . Eq. (5) demonstrates the minimum and maximum power generation limits.

To simplify the expressions, the solution is denoted as  $\mathbf{x}$  and the objective function is denoted as  $f(\cdot)$ . Since the DC-OPF problem is a linear programming problem, the constraints are represented by  $\mathbf{Ax} \leq \mathbf{b}$  in Sec. 3. Notably, the constraints for AC-OPF problems could also be addressed by the proposed MI-GAN if considering the constraints as  $g(\mathbf{x}) \leq \mathbf{b}$  instead.

### 3. RESEARCH METHODOLOGY

#### 1. Model-informed GAN (MI-GAN)

As illustrated in Figure 1, the MI-GAN is proposed to involve the OPF model in the training of GAN. It includes two key components, a model-informed (MI) generator  $G_m$  and a discriminator  $D$ . Based on the adversarial architecture in GAN,  $G_m$  will first generate the OPF solutions, and  $D$  will identify if the input solutions are generated or actual.  $G_m$  and  $D$  will compete until the distribution of generated solutions resembles the distribution of actual solutions. In this framework, the historical OPF solutions,  $\mathbf{X}_h$ , i.e., the optimal or near optimal solutions of the previous/solved OPF models, are considered as the actual solutions to feed  $D$ . Besides, a preserved matrix is also applied to save the generated solutions from the proposed MI-GAN, and this matrix is defined as saved solutions, i.e.,  $\mathbf{X}_s$ .

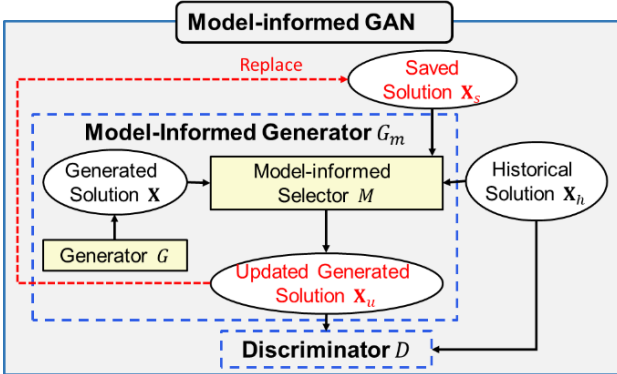


Figure 1. The overview of the proposed MI-GAN.

According to Eq. (1) in Sec. 1, the minimax game for the MI-GAN, i.e.,  $V(D, G_m)$ , can be formulated in Eq. (6),

$$\min_{G_m} \max_D V(D, G_m) = \mathbb{E}_{\mathbf{x}_h \sim P_{\text{data}}(\mathbf{x}_h)} [\log(D(\mathbf{x}_h))] + \mathbb{E}_{\mathbf{z} \sim P_{\mathbf{Z}}(\mathbf{z})} [\log(1 - D(G_m(\mathbf{z})))] \quad (6)$$

where  $\mathbf{x}_h$  is the historical solution while  $\mathbf{z}$  is the input noise for  $G_m$ . Accordingly, the loss of  $G_m$ , i.e.,  $L_{G_m}$ , and the loss of  $D$ ,  $L_D$ , could be demonstrated in Eq. (7).

$$L_{G_m} = -\mathbb{E}_{\mathbf{z} \sim P_{\mathbf{Z}}(\mathbf{z})} (D(G_m(\mathbf{z}))) \quad (7)$$

$$L_D = \mathbb{E}_{\mathbf{z} \sim P_{\mathbf{Z}}(\mathbf{z})} (D(G_m(\mathbf{z}))) - \mathbb{E}_{\mathbf{x}_h \sim P_{\text{data}}(\mathbf{x}_h)} (D(\mathbf{x}_h))$$

Specifically,  $G_m$  consists of a regular generator  $G$  and a newmodel-informed (MI) selector  $M$ . As shown in Eq. (8), in each training iteration,  $G$  will first generate solutions, i.e.,  $G(\mathbf{z})$ , and then it will be sent to  $M$ . Afterwards, according to the OPF constraints,  $M$  will select and update the feasible solutions among the generated solutions, based on the saved solution,  $\mathbf{X}_s$ , and historical solution  $\mathbf{X}_h$ .

$$G_m(\mathbf{z}) = M(G(\mathbf{z}) | \mathbf{X}_s, \mathbf{X}_h) \quad (8)$$

Subsequently, both  $\mathbf{X}_h$  and the selected generated solutions i.e.,  $\mathbf{X}_u$ , will be sent to  $D$ . Based on the output of  $D$ , the losses  $L_{G_m}$  and  $L_D$  could be obtained to update the model during iteration.  $\mathbf{X}_u$  will be saved and applied as  $\mathbf{X}_s$  in next iteration. In this way,  $\mathbf{X}_s$  and  $(D, G_m)$  can be further updated iteratively until it converges.

#### 2. Model-informed Selector

As mentioned in Sec. 3.1, the MI selector  $M$  is proposed to select and update the feasible solutions among the generated solutions. Hence, the feasibility of generated solutions should be checked first. Afterwards, the filtered feasible solutions are further updated based on the objective function values and the gradient information, respectively.

Accordingly, three different categories of new layers, including feasibility filter layer, comparison layer, and gradient-guided layer are proposed to establish  $M$  in  $G_m$ . The demonstration of  $M$  is shown in Figure 2.

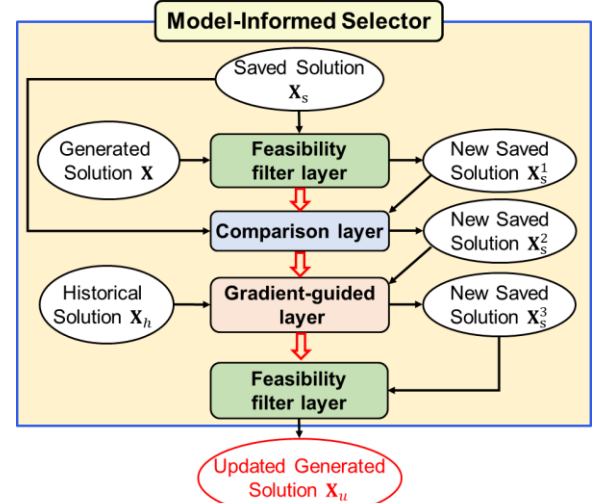


Figure 2. A demonstration of model-informed selector.

In Figure 2,  $M$  involves four steps to update the generated solutions. First, one feasibility filter layer is applied to check

whether the solutions satisfy the given OPF constraints, i.e., feasibility check. Then a comparison layer compares the objective function values based on the saved solutions and feasible generated solutions. Afterwards, the gradient-guided layer updates the solutions according to the available gradient information. Since the feasibility of updated solutions may not be guaranteed, one more feasibility layer is applied to determine if the updated solutions are still feasible.

### 1) Feasibility filter layer

The feasibility filter layer is to check if the input solutions satisfy the constraints. Two identical feasibility filter layers are needed in  $M$ . Figure 3(a) provides a framework overview of the feasibility filter layer. Initially, the generated solutions  $\mathbf{X}$  and saved solution  $\mathbf{X}_s$  are sent to this layer as pairs. One solution in the pair is a generated solution, while the other is a saved solution. Afterwards, each pair will select one solution to be passed to the updated saved solution set  $\mathbf{X}_s^1$ .

In particular, the  $i$ -th pair of generated solution and saved solution, i.e.,  $(\mathbf{X}^{(i)}, \mathbf{X}_s^{(i)})$ , may have four cases: i) feasible  $\mathbf{X}^{(i)}$  and infeasible  $\mathbf{X}_s^{(i)}$ ; ii) feasible  $\mathbf{X}^{(i)}$  and feasible  $\mathbf{X}_s^{(i)}$ ; iii) infeasible  $\mathbf{X}^{(i)}$  and infeasible  $\mathbf{X}_s^{(i)}$  also infeasible, as well as iv) infeasible  $\mathbf{X}^{(i)}$  and feasible  $\mathbf{X}_s^{(i)}$ . For case i) and iv), the feasible solution will be passed to the updated saved solution set  $\mathbf{X}_s^1$ . However, in case ii) and iii), the feasibility of the generated solution and saved solution is the same. Since the generated solution is obtained from  $G_m$  in current iteration, it is more representative than the saved solution to show the effectiveness of  $G_m$ . Hence, the generated solution should be passed to  $\mathbf{X}_s^1$  in case ii) and iii). In this way, under the first three cases, the generated solutions from  $\mathbf{X}$  will be passed to  $\mathbf{X}_s^1$ . Otherwise, the solutions from  $\mathbf{X}_s$  will be passed to  $\mathbf{X}_s^1$ . Notably, the feasibility of each pair  $(\mathbf{X}^{(i)}, \mathbf{X}_s^{(i)})$  is also recorded as a label, i.e., which feasibility case it belongs to, denoted as  $S_i$  ( $S_i = 1, 2, 3, 4$ ) in a label sequence  $S$ , and it will be sent to the comparison layer.

The algorithm for feasibility filter layer can be demonstrated by the Algorithm 1 below. For the  $i$ -th pair, only when  $\mathbf{X}^{(i)}$  is infeasible and  $\mathbf{X}_s^{(i)}$  is feasible,  $\mathbf{X}_s^{(i)}$  is passed to  $\mathbf{X}_s^1$  as  $\mathbf{X}_s^{1(i)}$ . Otherwise,  $\mathbf{X}^{(i)}$  is assigned as  $\mathbf{X}_s^{1(i)}$ . Thus, in each iteration, all the solutions in  $\mathbf{X}_s^1$  are essentially the generated solutions either synthesized from current iteration or previous iterations. In this way, the feasibility of the solutions which will be sent to  $D$  could be guaranteed. the feasibility of  $\mathbf{X}$  and  $\mathbf{X}_s$  is also recorded as labels in  $S$ , which will be applied in the comparison layer.

#### Algorithm 1: Feasibility filter algorithm

---

**Input:**  $\mathbf{X} \{ \mathbf{X}^{(1)}, \mathbf{X}^{(2)}, \dots, \mathbf{X}^{(n)} \}$ ,  $\mathbf{X}_s \{ \mathbf{X}_s^{(1)}, \mathbf{X}_s^{(2)}, \dots, \mathbf{X}_s^{(n)} \}$ ,  $\mathbf{A}$ ,  $\mathbf{b}$

**Step 1:** Define a new saved solution set as  $\mathbf{X}_s^1$

**For**  $i = 1$  **to**  $n$  **do**

- Step 2:** Calculate  $\mathbf{b} - \mathbf{AX}^{(i)}$
- Step 3:** Generate a  $n$ -element sequence  $S: \{0, 0, \dots, 0\}$
- If  $\mathbf{b} - \mathbf{AX}^{(i)} \leq \mathbf{0}$  and  $\mathbf{b} - \mathbf{AX}_s^{(i)} > \mathbf{0}$ :

  - Step 4:** Assign  $\mathbf{X}^{(i)}$  to  $\mathbf{X}_s^{1(i)}$  and set  $S_i = 1$
  - Else if  $\mathbf{b} - \mathbf{AX}^{(i)} \leq \mathbf{0}$  and  $\mathbf{b} - \mathbf{AX}_s^{(i)} \leq \mathbf{0}$ :

    - Step 5:** Assign  $\mathbf{X}^{(i)}$  to  $\mathbf{X}_s^{1(i)}$  and set  $S_i = 2$
    - Else if  $\mathbf{b} - \mathbf{AX}^{(i)} > \mathbf{0}$  and  $\mathbf{b} - \mathbf{AX}_s^{(i)} > \mathbf{0}$ :

      - Step 6:** Assign  $\mathbf{X}^{(i)}$  to  $\mathbf{X}_s^{1(i)}$  and set  $S_i = 3$
      - Else: Assign  $\mathbf{X}_s^{(i)}$  to  $\mathbf{X}_s^{1(i)}$  and set  $S_i = 4$

**Output**  $\mathbf{X}_s^1, S$

---

### 2) Comparison layer

The comparison layer is to compare the objective function values between  $\mathbf{X}_s^1$  and  $\mathbf{X}_s$ . Figure 3(b) depicts the framework of the comparison layer in  $M$ . Initially,  $\mathbf{X}_s^1$  and  $\mathbf{X}_s$  are also sent as pairs to the comparison layer. One solution in the pair is from  $\mathbf{X}_s^1$  while the other is from  $\mathbf{X}_s$ . Similar to the feasibility filter layer, each pair will select one solution to be passed to the newly saved solution set  $\mathbf{X}_s^2$ .

The  $i$ -th pair of generated solution and saved solution, i.e.,  $(\mathbf{X}_s^{1(i)}, \mathbf{X}_s^{(i)})$ , may have two cases, as shown in Eq. (9).

$$\text{i) } f(\mathbf{X}_s^{1(i)}) \geq f(\mathbf{X}_s^{(i)}); \text{ ii) } f(\mathbf{X}_s^{1(i)}) < f(\mathbf{X}_s^{(i)}). \quad (9)$$

Under such circumstances, a natural idea is to pass the solution with smaller objective function value to  $\mathbf{X}_s^2$ . However, the feasibility of  $\mathbf{X}$  and  $\mathbf{X}_s$  should also be considered in the comparison layer. Hence, case i) and ii) are discussed separately according to the feasibility of  $\mathbf{X}$  and  $\mathbf{X}_s$  to guarantee the feasibility of the output solutions:

- (a) For the case i), if  $\mathbf{X}_s^{(i)}$  is feasible, i.e.,  $S_i$  is 1 or 2,  $\mathbf{X}_s^{(i)}$  will be assigned as  $\mathbf{X}_s^{2(i)}$ ; Otherwise,  $\mathbf{X}_s^{1(i)}$  will be sent to  $\mathbf{X}_s^2$  as  $\mathbf{X}_s^{2(i)}$ .
- (b) For the case ii), only when  $\mathbf{X}_s^{1(i)}$  is feasible and  $\mathbf{X}_s^{(i)}$  is infeasible, i.e.,  $S_i$  is 1,  $\mathbf{X}_s^{(i)}$  will be assigned as  $\mathbf{X}_s^{2(i)}$ , Otherwise,  $\mathbf{X}_s^{1(i)}$  will be sent to  $\mathbf{X}_s^2$  as  $\mathbf{X}_s^{2(i)}$ .

Based on the above two cases, the algorithm for comparison layer is demonstrated in Algorithm 2 below. Two cases are considered separately with the help of calculated objective function values and  $S$ . In this way, the feasible solutions with smaller objective function values could be passed to  $\mathbf{X}_s^2$ .

---

#### Algorithm 2: Objective function value algorithm

---

**Input:**  $\mathbf{X}_s \{ \mathbf{X}_s^{1(1)}, \mathbf{X}_s^{1(2)}, \dots, \mathbf{X}_s^{1(n)} \}$ ,  $\mathbf{X}_s \{ \mathbf{X}_s^{(1)}, \mathbf{X}_s^{(2)}, \dots, \mathbf{X}_s^{(n)} \}$ ,  $\mathbf{c}, S$

**Step 1:** Define a new saved solution set as  $\mathbf{X}_s^2$

**For**  $i = 1$  **to**  $n$  **do**

**Step 2:** Calculate  $\mathbf{cX}_s^{1(i)}$  and  $\mathbf{cX}_s^{(i)}$

If  $\mathbf{cX}_s^{1(i)} < \mathbf{cX}_s^{(i)}$ :

If  $S_i = 1$ : Assign  $\mathbf{X}_s^{(i)}$  to  $\mathbf{X}_s^{2(i)}$ ; Else: Assign  $\mathbf{X}_s^{1(i)}$  to  $\mathbf{X}_s^{2(i)}$

Else if  $S_i > 2$ : Assign  $\mathbf{X}_s^{1(i)}$  to  $\mathbf{X}_s^{2(i)}$ ; Else: Assign  $\mathbf{X}_s^{(i)}$  to  $\mathbf{X}_s^{2(i)}$

**Output**  $\mathbf{X}_s^2$

---

### 3) Gradient-guided layer

The gradient-guided layer is to update the generated solutions according to the available gradient information. Figure 3(c) depicts the framework of the gradient-guided layer in  $M$ . Initially, this layer is fed by  $\mathbf{X}_s^2$  and historical solution  $\mathbf{X}_h$ , where both  $\mathbf{X}_s^2$  and  $\mathbf{X}_h$  have the same number of solutions. Hence,  $\mathbf{X}_s^2$  and  $\mathbf{X}_h$  are also combined as pairs in this layer. The  $i$ -th pair consists of the  $i$ -th solution of  $\mathbf{X}_s^2$ ,  $\mathbf{X}_s^{2(i)}$ , and the  $i$ -th solution of  $\mathbf{X}_h$ ,  $\mathbf{X}_h^{(i)}$ . Afterwards,  $\mathbf{X}_s^{2(i)}$  will be updated to  $\mathbf{X}_s^{3(i)}$  based on  $\mathbf{X}_h^{(i)}$ . Then  $\mathbf{X}_s^{3(i)}$  will be sent to the updated saved solution set  $\mathbf{X}_s^3$  as the  $i$ -th solution.

The solutions in  $\mathbf{X}_s^2$  are updated using gradient descent (GD) algorithm [21]. However, due to the complex formats of objective functions in OPF,  $\nabla f$  may be hard to calculate. Hence, for  $\mathbf{X}_s^{2(i)}$ ,  $\nabla f$  is estimated by calculating the slope between  $(\mathbf{X}_s^{2(i)}, f(\mathbf{X}_s^{2(i)}))$  and  $(\mathbf{X}_h^{(i)}, f(\mathbf{X}_h^{(i)}))$  in this work.

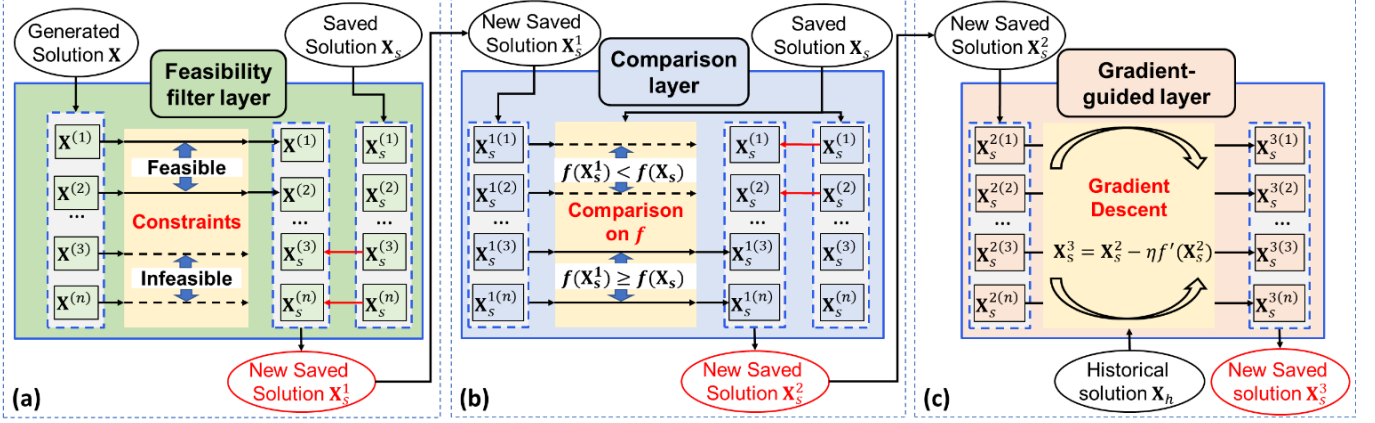


Figure 3. The framework of the feasibility filter layer (a), comparison layer (b), and gradient-guided layer (c) in the model-informed selector.

Afterwards, the step size of the GD algorithm is denoted as  $\eta$ , which could be determined through experimental trials. In this way, the solutions in  $\mathbf{X}_s^3$  could be updated toward the direction with smaller objective function values. Notably, the gradient-guided layer is not mandatory in MI-GAN but it could significantly accelerate the training process due to the guidance from gradient. Hence, MI-GAN will also work without this layer if the OPF model is highly complex and the gradient is hard to quantify.

In summary, based on the above-mentioned three new layers, the algorithm to implement  $M$  in  $G_m$  is demonstrated in Algorithm 3 below. The generated solution set  $\mathbf{X}$  is updated as  $\mathbf{X}_s^1$  in the first feasibility filter layer. Afterwards,  $\mathbf{X}_s^1$  is updated as  $\mathbf{X}_s^2$  in the comparison layer, and then  $\mathbf{X}_s^2$  is updated as  $\mathbf{X}_s^3$  in the gradient-guided layer. Finally,  $\mathbf{X}_s^3$  is updated as  $\mathbf{X}_u$  in the second feasibility filter layer. Notably, the input in the second feasibility filter layer are  $\mathbf{X}_s^3$  and  $\mathbf{X}_s^2$  rather than  $\mathbf{X}$  and  $\mathbf{X}_s$ . In this way,  $\mathbf{X}_u$  is considered as the output of model-informed selector. Thus, in each iteration, the generated solutions could be updated as feasible solutions towards the direction with smaller (i.e., better) objective function values.

#### Algorithm 3: Model-informed selector algorithm

**Input:**  $\mathbf{X} \{ \mathbf{X}^{(1)}, \mathbf{X}^{(2)}, \dots, \mathbf{X}^{(n)} \}$ ,  $\mathbf{X}_h \{ \mathbf{X}_h^{(1)}, \mathbf{X}_h^{(2)}, \dots, \mathbf{X}_h^{(m)} \}$ ,  $\mathbf{X}_s \{ \mathbf{X}_s^{(1)}, \mathbf{X}_s^{(2)}, \dots, \mathbf{X}_s^{(n)} \}$ ,  $\mathbf{c}$ ,  $\mathbf{A}$ ,  $\mathbf{b}$ , parameter  $\eta$ ,  $n$   
**Step 1:** Obtain  $\mathbf{X}_s^1$ ,  $S$  by sending  $\mathbf{X}$ ,  $\mathbf{X}_s$ ,  $\mathbf{A}$ ,  $\mathbf{b}$  to algorithm 1  
**Step 2:** Obtain  $\mathbf{X}_s^2$  by sending  $\mathbf{X}_s^1$ ,  $\mathbf{X}_s$ ,  $\mathbf{c}$ ,  $S$  to algorithm 2  
**Step 3:** Replicate  $\mathbf{X}_s^2$  as  $\mathbf{X}_s^3$   
**For**  $i = 1$  to  $n$  **do**  
**Step 4:** Calculate  $\mathbf{cX}_a^{(i)}$  and  $\mathbf{cX}_s^{2(i)}$   
**If**  $(\mathbf{cX}_s^{2(i)} - \mathbf{cX}_a^{(i)}) \leq 0$ :  
**Step 5:** Obtain  $\mathbf{X}_s^{3(i)} = \mathbf{X}_s^{2(i)} + \eta (f(\mathbf{X}_s^{2(i)}) - f(\mathbf{X}_a^{(i)})) / (\mathbf{X}_s^{2(i)} - \mathbf{X}_a^{(i)})$   
**Else:**  
**Step 6:** Obtain  $\mathbf{X}_s^{3(i)} = \mathbf{X}_s^{2(i)} - \eta (f(\mathbf{X}^{(i)}) - f(\mathbf{X}_a^{(i)})) / (\mathbf{X}_s^{2(i)} - \mathbf{X}_a^{(i)})$   
**Step 7:** Obtain  $\mathbf{X}_u$  by sending  $\mathbf{X}_s^3$ ,  $\mathbf{X}_s^2$ ,  $\mathbf{A}$ ,  $\mathbf{b}$  to algorithm 1  
**Output**  $\mathbf{X}_u$

### 3. Property of MI-GAN and its requirement

Based on the proposed MI-selector, the algorithm for MI-GAN is shown in Algorithm 4. The actual solution set, i.e., the historical solution set,  $\mathbf{X}_h$ , and the initialized saved solution set, i.e., the saved solution set  $\mathbf{X}_s$ , are sent to the MI-GAN. With the support of historical solutions, when  $L_D$  and  $L_{G_m}$  converge, the generated solutions should be similar to the historical solutions.

In addition, the objective function values of the saved solutions decrease with each iteration. In this way, the generated solutions could gradually approach the optimal solution.

#### Algorithm 4: MI-GAN algorithm

**Input:**  $\mathbf{X}_h \{ \mathbf{X}_h^{(1)}, \mathbf{X}_h^{(2)}, \dots, \mathbf{X}_h^{(m)} \}$ ,  $\mathbf{X}_s \{ \mathbf{X}_s^{(1)}, \mathbf{X}_s^{(2)}, \dots, \mathbf{X}_s^{(n)} \}$ ,  $\mathbf{c}$ ,  $\mathbf{A}$ ,  $\mathbf{b}$ ,  $f$ , parameter  $\eta$ ,  $n$   
**Repeat**  
**Step 1:** Randomly generate noise  $\mathbf{Z}$   
**Step 2:** Generate  $n$  fake solutions by generator as  $\mathbf{X} \{ \mathbf{X}^{(1)}, \mathbf{X}^{(2)}, \dots, \mathbf{X}^{(n)} \}$   
**Step 3:** Obtain  $\mathbf{X}_u$  by inputting  $\mathbf{X}_h$ ,  $\mathbf{c}$ ,  $\mathbf{A}$ ,  $\mathbf{b}$ ,  $f$  to algorithm 3  
**Step 4:** Send  $\mathbf{X}_h$  and  $\mathbf{X}_u$  into discriminator  $D$  to get output label results  $D(\mathbf{X})$  and  $D(\mathbf{Z})$ , respectively  
**Step 5:** Optimize the model parameters based on the output of discriminator  
**Step 6:** Assign  $\mathbf{X}_u$  to  $\mathbf{X}_s$   
**Until** both the  $Loss_{G_m}$ ,  $-D(\mathbf{X})$ , and  $Loss_D$ ,  $D(\mathbf{X}) - D(\mathbf{Z})$ , converge  
**Output**  $G_m$ ,  $D$

In the MI-GAN, the initialization requires to pre-define the saved solution set in the first iteration. Under such circumstances, an initialized saved solution set is considered, among which each solution is set as a vector with extremely large values. In this way, based on the feasibility layer and comparison layer, the initialized saved solution set could be replaced by the generated solutions in the first iteration. Then in the following iterations, all the solutions in  $\mathbf{X}_s$  are the generated solutions from MI-GAN, either synthesized from current iteration or previous iterations. Hence, the initialized saved solutions will not interfere the update of MI-GAN.

It is worth noting that MI-GAN can also work well even if the historical solutions are not available. If there are no historical solutions, with the given OPF problem, sampling from the feasible region could be applied to obtain the feasible solutions, which could be considered as actual solutions. However, in the large-scale OPF models, the sampling for feasible solutions may take a long time. Under such circumstances, in order to reduce the sampling time, the constraints could be partially relaxed. The case studies in Sec. 4 will show that the proposed method can still work well with the relaxed constraints.

Considering that the proposed MI-generator,  $G_m$ , is employed, it is also essential to prove that, as shown in Proposition 1, the convergence property is similar to GAN.

**Proposition 1.** The convergence property of MI-GAN is similar to GAN, i.e., when  $P_{\text{data}} = P_Z$  [14], it will converge.

**Proof.** Actual solutions are from the distribution of historical solutions,  $P_{\text{data}}$ , while the artificial solutions are from another distribution,  $P_Z$ . When  $G_m$  is fixed, the optimal discriminator  $D$  can be shown as

$$D_G^*(\mathbf{x}) = \frac{P_{\text{data}}(\mathbf{x})}{P_{\text{data}}(\mathbf{x}) + P_Z(\mathbf{x})} \quad (10)$$

Then the minimax game when  $G_m$  is fixed is reformulated as

$$\begin{aligned} \max_D V(D, G_m) &= \mathbb{E}_{\mathbf{x} \sim P_{\text{data}}(\mathbf{x})} \left[ \frac{P_{\text{data}}(\mathbf{x})}{P_{\text{data}}(\mathbf{x}) + P_Z(\mathbf{x})} \right] \\ &\quad + \mathbb{E}_{\mathbf{x} \sim P_Z(\mathbf{x})} \left[ \frac{P_Z(\mathbf{x})}{P_{\text{data}}(\mathbf{x}) + P_Z(\mathbf{x})} \right] \end{aligned} \quad (11)$$

Afterwards, only when  $P_{\text{data}} = P_Z$ , the global minimum value of  $\max_D V(D, G_m)$  shown in Eq. (11) can be achieved [14].

In this way, the distribution of the generated solutions will gradually approach to the distribution of the historical solutions.

Q.E.D.

Based on the convergence property,  $P_Z$ , should be similar to  $P_{\text{data}}$ . Denote that the optimal solution is  $\mathbf{x}^*$ . Hence, if  $\mathbf{x}^*$  locates in  $P_{\text{data}}$ , the generated solutions from  $G_m$ , i.e.,  $\mathbf{X}$ , should be around  $\mathbf{x}^*$ . Following that, the solution with the smallest objective function values among  $\mathbf{X}$  could be selected as the output solution from the MI-GAN model.

However, if  $\mathbf{x}^*$  does not locate in  $P_{\text{data}}$ ,  $\mathbf{X}$  may not be around  $\mathbf{x}^*$ . Hence, a new algorithm to improve the training of MI-GAN called recursive iteration algorithm, is being developed in Sec. 3.4 to address this issue.

#### 4. Recursive Iteration Algorithm

As described in Sec. 3.3, when the historical solutions  $\mathbf{X}_a$  are not available, the sampled actual feasible solutions applied to train the MI-GAN may be far away from  $\mathbf{x}^*$ . Denote such actual solution set as  $\mathbf{X}_a$ . Though the MI-GAN converges, the generated solutions  $\mathbf{X}$  probably are still not close enough to  $\mathbf{x}^*$ . Under such circumstances, it is important to make sure that the generated solutions  $\mathbf{X}$  will approach to  $\mathbf{x}^*$ . Hence, as shown in Figure 4, a recursive iteration algorithm for MI-GAN update is proposed to gradually bring  $\mathbf{X}$  closer to  $\mathbf{x}^*$ . Since  $\mathbf{X}$  are similar to  $\mathbf{X}_a$ , a natural idea is to select the solutions with smallest objective function values from both  $\mathbf{X}$  and  $\mathbf{X}_a$ . Such updated solutions, namely,  $\mathbf{X}'_a$ , should be closer to  $\mathbf{x}^*$  than  $\mathbf{X}_a$ .

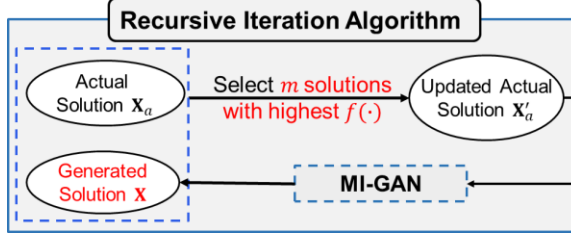


Figure 4. The framework of the recursive iteration algorithm.

Afterwards,  $\mathbf{X}'_a$  are applied to continue the training for MI-GAN until the losses converge again. In this way, each loop, which could be considered as one recursive iteration, will make newly generated solutions closer to  $\mathbf{x}^*$  than the previously generated solutions. To further demonstrate the effectiveness of the recursive iteration, the proposition 2 is presented below.

**Proposition 2.** Denote that the output solution from the  $k$ -th trained MI-GAN with the smallest  $f(\mathbf{x})$  is  $\hat{\mathbf{x}}_k$ . Then  $\hat{\mathbf{x}}_k$  will not be worse than  $\hat{\mathbf{x}}_{k-1}$ . That is,

$$f(\hat{\mathbf{x}}_k) \leq f(\hat{\mathbf{x}}_{k-1}) \quad (12)$$

**Proof.** Denote that the actual solution set and generated solution set of the  $k$ -th trained MI-GAN is  $\mathbf{X}_{a_k}$  and  $\mathbf{X}_k$ . According to Figure 4,  $\mathbf{X}_{a_k}$  are selected among  $\mathbf{X}_{a_{k-1}}$  and  $\mathbf{X}_{k-1}$ . Since the selection principle is to compare the objective function values,  $\mathbf{X}_{a_k}$  is better than  $\mathbf{X}_{a_{k-1}}$ . Therefore, for any solution  $\mathbf{x}_k$  from  $\mathbf{X}_{a_k}$ , there must exist at least one solution  $\mathbf{x}_{k-1}$  from  $\mathbf{X}_{a_{k-1}}$  such that  $f(\mathbf{x}_k) \leq f(\mathbf{x}_{k-1})$ .

Q.E.D.

Based on proposition 2, more importantly, to show the converge property of the proposed recursive iteration algorithm for MI-GAN, the proposition 3 is obtained below as well.

**Proposition 3.**  $\hat{\mathbf{x}}_k$  will gradually converge to optimal solution  $\mathbf{x}^*$  as  $k$  increases.

**Proof.** Due to proposition 2,  $f(\hat{\mathbf{x}}_k)$  monotonically decreases as  $k$  increases. In addition,  $f(\hat{\mathbf{x}}_k)$  is bounded by  $f(\mathbf{x}^*)$ . Hence, according to the monotone convergence theorem [22],  $\hat{\mathbf{x}}_k$  could converge to  $\mathbf{x}^*$  as  $k$  increases.

Q.E.D.

In practice, since the optimal solution is unknown, it is critical to define the stopping criteria for the recursive iteration algorithm. Due to the gradient-guided layer, the output solutions of MI-GAN will typically outperform  $\mathbf{X}_a$ . Then Eq. (13) could be satisfied in most recursive iterations, which will make  $\hat{\mathbf{x}}_k$  gradually approach to  $\mathbf{x}^*$ .

However, when  $\hat{\mathbf{x}}_k$  is around  $\mathbf{x}^*$ , then Eq. (13) may not be satisfied. Hence, based on Eq. (13), the stopping criteria could be developed as follows: if  $f(\hat{\mathbf{x}}_k)$  does not decrease in next two consecutive iterations, i.e., no better solutions, the iterative process will be terminated.

$$|\mathbf{x}^* - \hat{\mathbf{x}}_k| \leq |\mathbf{x}^* - \hat{\mathbf{x}}_{k-1}| \quad (13)$$

According to Figure 4 and the stopping criteria, the pseudo code for the recursive iteration algorithm is demonstrated in Algorithm 5 below. In each iteration, the MI-GAN is trained according to  $\mathbf{X}_a$  and generate  $\mathbf{X}$  after model converges. Then  $m$  solutions are selected as  $\mathbf{X}'_a$  among  $\mathbf{X}_a$  and  $\mathbf{X}$ .  $\mathbf{X}'_a$  is applied in next recursive iteration, and iteration will be terminated based on the proposed stopping criteria. In this way, this recursive iteration algorithm could help to find solution close to optimal.

---

**Algorithm 5:** Recursive iteration algorithm

---

**Input:**  $\mathbf{X}_a \{\mathbf{X}_a^{(1)}, \mathbf{X}_a^{(2)}, \dots, \mathbf{X}_a^{(m)}\}$ , parameter  $\delta, h$

**Step 1:** Set  $k = 1$

**Loop**

**Step 2:** Train MI-GAN by  $\mathbf{X}_a$

**Step 3:** Generate  $h$  artificial samples  $\mathbf{X}$  from the trained MI-GAN

**Step 4:** Select  $m$  solutions with smallest objective function value as  $\mathbf{X}'_a$  among  $\mathbf{X}_a$  and  $\mathbf{X}$

**Step 5:** Assign  $\mathbf{X}'_a$  to  $\mathbf{X}_a$

**Step 6:** Calculate the minimum objective function value of  $\mathbf{X}_a$ ,  $f_{\min}^k$  and its output solution  $\hat{\mathbf{x}}_k$

**Step 7:**  $k = k + 1$

**Until**  $f_{\min}^{k-2} \leq f_{\min}^{k-1}$  and  $f_{\min}^{k-2} \leq f_{\min}^k$ :

**Output**  $f_{\min}^{k-2}$  and  $\hat{\mathbf{x}}_{k-2}$

---

## 4. CASE STUDIES

### 1. Data Introduction and Experimental Setup

The experimental setups in this work are similar to those in Venzke *et al.* [23], and six DC-OPF cases are demonstrated. The detailed setup of each case is shown in TABLE I. Notably, the case 9 is from the MATPOWER [24]. As the number of buses, i.e.,  $n_b$ , increases from 9 to 162, so does the number of constraints, from 24 to 592. Due to the significantly different scale of the cases, it could demonstrate the effectiveness of the proposed method comprehensively.

TABLE I: Experiment Setup for DC-OPF cases

Setup	Cases					
	Case 9	Case 30	Case 39	Case 57	Case 118	Case 162
$n_b$	9	30	39	57	118	162
$n_g$	3	2	10	4	19	12
$n_d$	3	21	21	42	99	113
$n_{line}$	9	41	46	80	186	284
Max. loading	315.0 MW	283.4 MW	6254.2 MW	1250.8 MW	4242.0 MW	7239.1 MW
Constraints	24	86	112	168	410	592
Relaxed Constraints	0	0	6	1	19	49

In order to obtain the sampled actual solutions for the proposed method as the input, 3,000 feasible solutions are initially sampled for each case before training the proposed method. In the sampling process,  $\mathbf{p}_g$  is first uniformly sampled from the range defined in Eq. (5). Afterwards,  $\boldsymbol{\theta}$  is calculated based on Eq. (3) and sent to Eq. (4) for feasibility check.

As  $n_b$  increases in each case, the difficulty of sampling the feasible solutions also increases, resulting in a significantly increase of sampling time. Besides, it will also be more difficult to synthesize feasible solutions in the proposed method. Hence, to reduce the sampling time and the difficulties to obtain sufficient feasible solutions, the number of constraints could be randomly relaxed as the number of variables is relatively large. The number of relaxed constraints for each case is also shown in TABLE I..

Notably, the proposed MI-GAN is compatible with most of the popular GAN architectures. In this study, MI-GAN is built by incorporating the popular Wasserstein GAN (WGAN) [25] since WGAN could make the training process more stable than the conventional GAN. Besides, the multilayer perceptron (MLP) network is applied in both generator and discriminator of the proposed MI-GAN. All above cases have the same parameter setups when using the proposed MI-GAN. The generator consists of five fully connected layer, whereas the discriminator consists of three fully connected layer. The last layer in the generator does not use the activation function while all the other layers incorporate Leaky\_ReLU as the activation function. TensorFlow 1.13 [26] is applied for the training of the proposed method. The batching size is set as 50 while the number of iterations is set as 2,000. Each case involves five trials. In each trial, the output is one feasible solution with the smallest objective function value. Afterwards, the mean of the output solutions from different trials are calculated for

discussion. The experiments were conducted on a laptop with i7-9750H CPU @2.60 GHz, 16 GB RAM.

According to Eq. (3) in Sec. 2, if  $\mathbf{p}_g$  is obtained,  $\boldsymbol{\theta}$  could also be calculated. Hence, to simplify the generation process of feasible solutions,  $\mathbf{p}_g$  is generated in the generator of the proposed method instead of  $\{\mathbf{p}_g, \boldsymbol{\theta}\}$ . Then prior to passing the variables to the layers in the model-informed selector,  $\boldsymbol{\theta}$  is initially calculated. In this way, the discriminator in the proposed MI-GAN will still distinguish the entire solution.

In this study, to demonstrate the effectiveness of the proposed method comprehensively, two different scenarios are considered. Sec. 4.2 showed the performance of MI-GAN for a given fixed OPF problems while Sec. 4.3 showed the performance of MI-GAN for the OPF problem with uncertainties.

### 2. MI-GAN performance for given fixed OPF problems

The performance of the proposed MI-GAN for the six given cases is shown in TABLE II. In this study, under each case, the feasible solution generated from the MI-GAN with the smallest objective function value is considered as its output solution. The accuracy of the output solution is measured by mean square errors (MAE) in percentage from the objective function values of the output solution and the actual optimal solution. The MAEs for different cases are shown in the first row of TABLE II, with the values in the brackets representing the standard deviations. Based on the MAEs, it is shown that the bias between the optimal objective function values from MI-GAN and the actual optimal objective function value could be less than 5% in most cases. Specifically, under the case30 and case57, the bias of the objective function values from the proposed method could be less than 1%. For case162, it is worth noting that the distance between the output solution of MI-GAN and the optimal solution does not increase compared with the distance calculated under other cases. Hence, though the MAE calculated under case162 is greater than 5%, it is still comparable. Therefore, the proposed method's output solutions are very close to the actual optimal solutions, demonstrating the method's effectiveness. Besides, the standard deviations under each case are less than 3%. Hence, it shows that the proposed method could generate the desired solutions accurately and consistently.

TABLE II  
Performance of the proposed method for DC-OPF cases

Results	Cases					
	Case 9	Case 30	Case 39	Case 57	Case 118	Case 162
MAE (%)	4.5 (2.9)	0.06 (0.3)	4.7 (1.6)	0.8 (0.4)	4.0 (2.6)	9.4 (2.0)
Recursive iterations	2.8 (1.6)	1.2 (0.4)	1.4 (0.5)	2.4 (0.5)	1.6 (0.8)	3.8 (1.9)
Running time	7.73 (0.08)	8.73 (0.27)	9.30 (0.32)	9.65 (0.44)	13.56 (0.67)	15.78 (0.12)

In addition, to demonstrate the effectiveness of the proposed recursive iteration algorithm, the number of recursive iterations is also shown in TABLE II, where the values in the brackets are also the standard deviations. Except for case162, all cases could obtain near-optimal solutions within three recursive iterations.

Though the number of recursive iterations in case162 is slightly larger, it is still less than four, which is comparable. Hence, it shows that the recursive iteration algorithm is beneficial and essential to improve MI-GAN.

Besides, the experimental running time of MI-GAN were also recorded to demonstrate the efficiency for the proposed method for use in the online power systems. Specifically, the running time for one recursive iteration in each case is collected from five replicates, and the average running time is calculated. The running time and its standard deviations of the proposed method are also shown in TABLE II. The running time will gradually increase as the number of variables increases, owing to the matrix calculations in the model-informed selector becoming increasingly complex.

Furthermore, the running time of the classical simplex algorithm [27] for solving the same OPF models is also calculated and compared to better demonstrate the efficiency of MI-GAN. The comparisons are demonstrated in Figure 5(a)-(b). Figure 5(a) depicts the average running time and the fitted curve of running time for both approaches. Due to the incorporation of neural networks, the proposed method takes longer to run than the simplex method. However, as shown in Figure 5(a), since  $R^2$  of fitted running time curve for both approaches are greater than 90%, the equations to demonstrate the running time for both approaches are convincing. Hence, the running time of the proposed MI-GAN increases linearly while the running time of simplex method increases exponentially. As the number of variables increases to a larger scale, the running time of proposed method can be more competitive than the simplex method. In addition, the slopes of running time for both approaches, as shown in Figure 5(b), can better demonstrate the increasing trend of running time. The slope of the proposed method fluctuates whereas the slope of simplex method increases. In case162, the slope of simplex method exceeds the slope of the proposed method. Hence, the proposed method may have a significantly shorter running time than the simplex method for large-scale cases. Since the proposed method could still obtain near optimal solutions, the proposed method has the fully potential to be applied in large-scale power systems.

### 3. Performance for OPF problem with uncertainties

#### 1) Solution accuracy

Given that the renewable energy intermittency may disturb power system stability, it is also important to demonstrate the robustness of the proposed method to address the environmental uncertainty. Hence, the experiments to add the fluctuations to the net loads are conducted, in which case9 and case57 are applied. The experiments are designed as follows: the proposed method is initially trained given the original net loads,  $\mathbf{p}_d$ . After the proposed method converges, the net loads are changed to  $\rho\mathbf{p}_d$ . Under the net loads of  $\rho\mathbf{p}_d$ , the feasible region will change and the optimal solution will be updated as  $\mathbf{x}^{* \prime}$ , resulting in the updated objective function value, i.e.,  $f(\mathbf{x}^{* \prime})$ . Afterwards, the MI-GAN is trained based on the changed net loads, and new output solution of MI-GAN should be obtained. If the proposed method is effective and robust, the

objective function value calculated by the new output solution should still be similar as  $f(\mathbf{x}^{* \prime})$ .

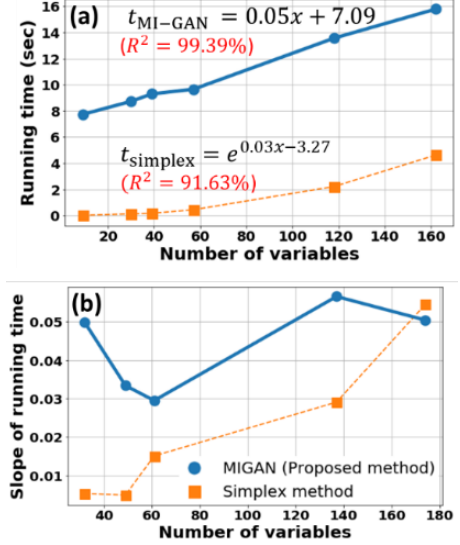


Figure 5. The comparison of the proposed method and simplex method for running time (a) and the slope of running time (b).

To better demonstrate the performance of the proposed method, a benchmark approach based on the DNN regression [10] and conventional GAN [14], which has been applied in several existing related studies, is selected to compare with the proposed MI-GAN. To make the comparison convincing, the network structure of the benchmark method is optimized as well. Specifically, in the benchmark method, MLP is also applied in both  $D$  and  $G$ . Through hyper-parameter tuning,  $G$  involves two fully-connected hidden layers while  $D$  involves only one fully-connected hidden layer.

Since the feasible regions for both the proposed method and the benchmark method may change as the net loads change, the applied actual data may be neither feasible nor close to the optimal solution. Hence, when the net loads change, 1000 solutions that adhere to the updated constraints are sampled. Then, they will be added to the existing actual data to train the model. To fully show the capability of MI-GAN, two cases that change the net loads in two different directions are considered, which are listed as follows:

- Increasing the net loads  $\mathbf{p}_d$  and  $\rho$  is selected among the set  $\{1.05, 1.1, 1.15, 1.2, 1.25, 1.3, 1.4, 1.5\}$ .
- Decreasing the net loads  $\mathbf{p}_d$  and  $\rho$  is selected among the set  $\{0.5, 0.6, 0.7, 0.75, 0.8, 0.85, 0.9, 0.95\}$ .

The MAEs and standard deviations of the proposed method and the benchmark approach for case9 are shown in Figure 6(a)-(d). The benchmark approach may have lower MAEs than the proposed method at the beginning when both increasing and decreasing the net loads. However, the MAEs of the benchmark approach will gradually increase and become larger than those of the proposed method as  $|1 - \rho|$  increases. Hence, it shows that the proposed method is more robust than the benchmark approach. In addition, the benchmark approach's standard deviations are generally higher than those of the proposed method, and increase as  $|1 - \rho|$  increases, while the standard deviations of the proposed MI-GAN remain similar. The comparisons among standard deviations also reveal that the

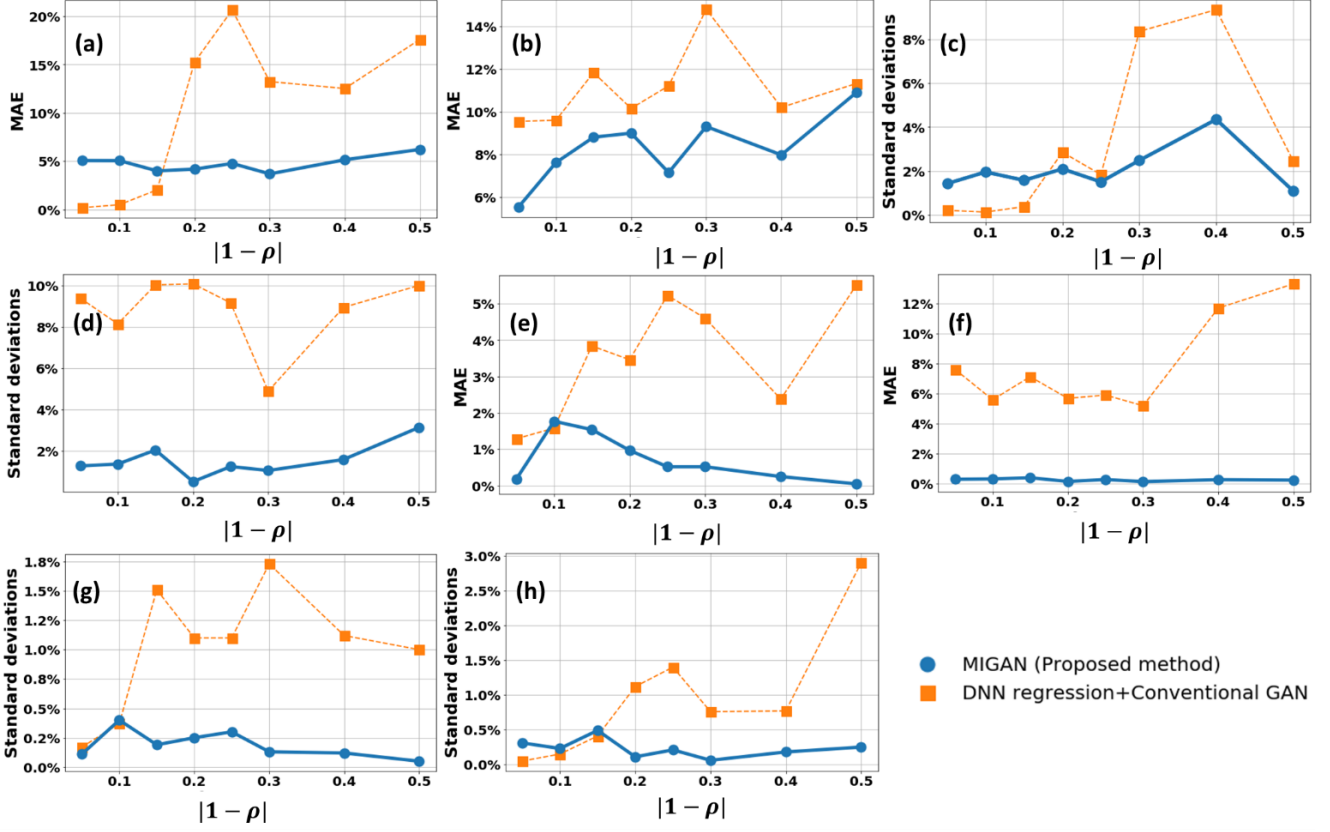


Figure 6. The comparison between the proposed method and DNN regression + Conventional GAN when increasing and decreasing the net loads for case9 (a-d) and case57 (e-h): (a) MAE when increasing the net loads under case9; (b) MAE when decreasing the net loads under case9; (c) standard deviations of MAE when increasing the net loads under case 9; (d) standard deviations of MAE when decreasing the net loads under case 9; (e) MAE when increasing the net loads under case57; (f) MAE when decreasing the net loads under case57; (g) standard deviations of MAE when increasing the net loads under case57; (d) standard deviations of MAE when decreasing the net loads under case57.

proposed method has higher stability than the benchmark approach.

On the other hand, the MAEs and standard deviations of the proposed method and the benchmark approach for case57 are shown in Figure 6(e)-(h). It is obviously shown that the MAEs of the benchmark approach will gradually increase and be larger than the proposed method regardless of whether the net loads are increased or decreased. Furthermore, the MAEs and the standard deviations of the proposed method do not show any significantly increasing or decreasing as  $|1 - \rho|$  increases. Therefore, the proposed method also outperforms the benchmark method under case57. Overall, the experiments conducted under both case9 and case57 demonstrate that the proposed method is not sensitive to the dynamic changes of power systems. Even if the coefficients change, the trained MIGAN could still be applied and find the near optimal solutions effectively.

## 2) Needed recursive iterations

Since the proposed method employs the recursive iteration algorithm, it is also necessary to discuss the changes of recursive iterations as the power systems interfere. The number of recursive iterations for case9 and case57 are shown in Figure 7(a)-(b). For both case9 and case57, the number of recursive iterations is mostly around 2 to 5, and it does not change significantly as  $|1 - \rho|$  increases. Hence, it shows the high robustness of the proposed method. Furthermore, despite the fact that the benchmark approach is optimized and has less

layers than the proposed method, the benchmark approach runs in about 55 seconds in both cases 9 and 57. Compared with the running time of the proposed method in TABLE II, the proposed method still outperforms the benchmark approach in terms of efficiency. Therefore, the experiments with different net loads fully demonstrate the superior performance of the proposed method and its highly potential to be applied in the large-scale OPF problems under uncertainty.

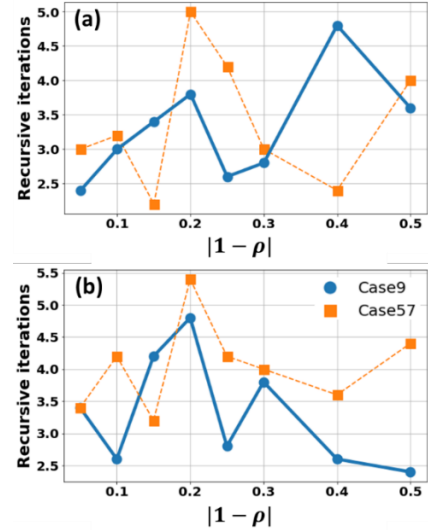


Figure 7. The number of recursive iterations when changing the net loads under case9 and case57: (a) the number of recursive iterations when increasing the net loads; (b) the number of recursive iterations when decreasing the net loads.

## 5. CONCLUSIONS

In this paper, a novel MI-GAN framework is proposed to address the OPF problem under net load uncertainty. In comparison to the existing optimization models, the proposed MI-GAN has three major contributions: (i) three important new layers, including the feasibility filter layer, comparison layer, and gradient-guided layer, are proposed and designed to ensure the feasibility and improve the optimality of generated solutions; (ii) an efficient MI selector in conjunction with the three new layers are developed, incorporating the GAN-based architecture as an important component of the generator, i.e., MI-generator; and (iii) a new recursive iteration algorithm is also proposed to further reduce the bias between selected solutions and optimal solutions. It is also worth noting that the proposed MI-GAN framework is compatible with most of the popular GAN architectures, which could further improve its capability of solving different optimization problems in power systems.

The superior performance of MI-GAN is demonstrated by six DC-OPF cases, including case9, case30, case37, case57, case118, case162. Among these six cases, the MAEs between the objective function values obtained from the proposed method and the actual optimal objective function value demonstrate the effectiveness of the proposed MI-GAN. In addition, the running times of the proposed method are also discussed to show its potential of computational efficiency. The running time increases linearly as the number of variables increases, showing that the proposed MI-GAN is more efficient than the conventional optimization techniques in solving large-scale OPF problems. Furthermore, to demonstrate its capability of handling uncertainties in power system, the experiments with increasing and decreasing net loads are also conducted under case9 and case57. The lower MAEs of the proposed method than the benchmark approach demonstrate that the proposed method is effective to handle the power system dynamics. The relatively low standard deviations and relatively stable number of recursive iterations also show the high robustness of the proposed method. Therefore, the proposed MI-GAN is very promising for finding the optimal solutions of the complex larger-scale OPF-related problems.

## 6. REFERENCES

- [1] Outlook, A. E. (2009). DOE/EIA-0383. Energy Information Administration, US Department of Energy, Washington, DC.
- [2] Yong, T., & Lasseter, R. H. (2000, July). Stochastic optimal power flow: formulation and solution. In *2000 Power Engineering Society Summer Meeting (Cat. No. 00CH37134)* (Vol. 1, pp. 237-242). IEEE.
- [3] Kimball, L. M., Clements, K. A., Pajic, S., & Davis, P. W. (2003, June). Stochastic OPF by constraint relaxation. In *2003 IEEE Bologna Power Tech Conference Proceedings*, (Vol. 4, pp. 5-pp). IEEE.
- [4] Delage, E., & Ye, Y. (2010). Distributionally robust optimization under moment uncertainty with application to data-driven problems. *Operations research*, 58(3), 595-612.
- [5] Martinez-Mares, A., & Fuerte-Esquivel, C. R. (2013). A robust optimization approach for the interdependency analysis of integrated energy systems considering wind power uncertainty. *IEEE Transactions on Power Systems*, 28(4), 3964-3976.
- [6] Zhang, Y., Shen, S., & Mathieu, J. L. (2016). Distributionally robust chance-constrained optimal power flow with uncertain renewables and uncertain reserves provided by loads. *IEEE Transactions on Power Systems*, 32(2), 1378-1388.
- [7] Guo, Y., Baker, K., Dall'Anese, E., Hu, Z., & Summers, T. H. (2018). Data-based distributionally robust stochastic optimal power flow—Part I: Methodologies. *IEEE Transactions on Power Systems*, 34(2), 1483-1492.
- [8] Yang, K., Gao, W., & Fan, R. (2021, November). Optimal Power Flow Estimation Using One-Dimensional Convolutional Neural Network. In *2021 North American Power Symposium (NAPS)* (pp. 1-6). IEEE.
- [9] Jia, Y., & Bai, X. (2021, August). A CNN approach for optimal power flow problem for distribution network. In *2021 Power System and Green Energy Conference (PSGEC)* (pp. 35-39). IEEE.
- [10] Falconer, T., & Mones, L. (2020). Deep learning architectures for inference of AC-OPF solutions. *arXiv preprint arXiv:2011.03352*.
- [11] Owerko, D., Gama, F., & Ribeiro, A. (2020, May). Optimal power flow using graph neural networks. In *ICASSP 2020-2020 IEEE International Conference on Acoustics, Speech and Signal Processing (ICASSP)* (pp. 5930-5934). IEEE.
- [12] Yan, Z., & Xu, Y. (2020). Real-time optimal power flow: A lagrangian based deep reinforcement learning approach. *IEEE Transactions on Power Systems*, 35(4), 3270-3273.
- [13] Zhou, Y., Zhang, B., Xu, C., Lan, T., Diao, R., Shi, D., ... & Lee, W. J. (2020). A data-driven method for fast ac optimal power flow solutions via deep reinforcement learning. *Journal of Modern Power Systems and Clean Energy*, 8(6), 1128-1139.
- [14] Goodfellow, I., Pouget-Abadie, J., Mirza, M., Xu, B., Warde-Farley, D., Ozair, S., ... & Bengio, Y. (2014). Generative adversarial nets. In *Advances in neural information processing systems* (pp. 2672-2680).
- [15] Tanaka, F. H. K. D. S., & Aranha, C., "Data Augmentation Using GANs," *arXiv preprint arXiv:1904.09135*, 2019.
- [16] Li, Y., Shi, Z., Liu, C., Tian, W., Kong, Z., & Williams, C. B. (2021). Augmented Time Regularized Generative Adversarial Network (ATR-GAN) for Data Augmentation in Online Process Anomaly Detection. *IEEE Transactions on Automation Science and Engineering*.
- [17] Fiore, U., De Santis, A., Perla, F., Zanetti, P., & Palmieri, F. (2017). "Using generative adversarial networks for improving classification effectiveness in credit card fraud detection," *Information Sciences*, 479, 448-455.
- [18] Liu, Y., Zhou, Y., Liu, X., Dong, F., Wang, C., & Wang, Z., "Wasserstein GAN-based small-sample augmentation for new-generation artificial intelligence: A case study of cancer-staging data in biology," *Engineering*, 5(1), 156-163, 2019.
- [19] Radford, A., Metz, L., & Chintala, S. (2015). Unsupervised representation learning with deep convolutional generative adversarial networks. *arXiv preprint arXiv:1511.06434*.
- [20] Douzas, G., & Bacao, F. (2018). Effective data generation for imbalanced learning using conditional generative adversarial networks. *Expert Systems with applications*, 91, 464-471.
- [21] Ruder, S. (2016). An overview of gradient descent optimization algorithms. *arXiv preprint arXiv:1609.04747*.
- [22] Kolmogorov, A. N., & Fomin, S. V. (1957). *Elements of the theory of functions and functional analysis* (Vol. 1). Courier Corporation.
- [23] Venzke, A., Qu, G., Low, S., & Chatzivasileiadis, S. (2020, November). Learning optimal power flow: Worst-case guarantees for neural networks. In *2020 IEEE International Conference on Communications, Control, and Computing Technologies for Smart Grids (SmartGridComm)* (pp. 1-7). IEEE.
- [24] R. D. Zimmerman, C. E. Murillo-Sánchez and R. J. Thomas, "Mat-power: Steady-state operations planning and analysis tools for power systems research and education", *IEEE Transactions on power systems*, 26(1), 12-19.
- [25] Arjovsky, M., Chintala, S., & Bottou, L. (2017). Wasserstein gan. *arXiv* 2017. *arXiv preprint arXiv:1701.07875*, 30, 4.
- [26] Abadi, M., Barham, P., Chen, J., Chen, Z., Davis, A., Dean, J., ... & Zheng, X. (2016). {TensorFlow}: A System for {Large-Scale} Machine Learning. In *12th USENIX symposium on operating systems design and implementation (OSDI 16)* (pp. 265-283).
- [27] Dantzig, G. B. (1990). Origins of the simplex method. In *A history of scientific computing* (pp. 141-151).